Intensification of Convective Heat Transfer in a Stator–Rotor–Stator Spinning Disc Reactor

Michiel M. de Beer, Jos T.F. Keurentjes, Jaap C. Schouten, and John van der Schaaf
Laboratory of Chemical Reactor Engineering, Dept. of Chemical Engineering and Chemistry, Eindhoven University of Technology, P.O. Box 513, 5600 MB, Eindhoven, The Netherlands

DOI 10.1002/aic.14788
Published online March 30, 2015 in Wiley Online Library (wileyonlinelibrary.com)

A stator–rotor–stator spinning disc reactor is presented, which aims at intensification of convective heat-transfer rates for chemical conversion processes. Single phase fluid-rotor heat-transfer coefficients h_r are presented for rotor angular velocities $\omega=0-157$ rad s^{-1} and volumetric throughflow rates $\phi_v=15-20 \cdot 10^{-6}$ m^3s^{-1}. The values of h_r are independent of ϕ_v and increase from 0.95 $kWm^{-2}K^{-1}$ at $\omega = 0$ rad s^{-1} to 34 $kWm^{-2}K^{-1}$ at $\omega = 157$ rad s^{-1}. This is a factor 2–3 higher than values achievable in passively enhanced reactor-heat exchangers, due to the 1–2 orders of magnitude larger specific energy input achievable in the stator–rotor–stator spinning disc reactor. Moreover, as h_r is independent of ϕ_v, the heat-transfer rates are independent of residence time. Together with the high mass-transfer rates reported for rotor–stator spinning disc reactors, this makes the stator–rotor–stator spinning disc reactor a promising tool to intensify heat-transfer rates for highly exothermal chemical reactions. *AIChE J*, 61: 2307–2318, 2015
Keywords: spinning disc reactor, convective heat-transfer, rotor–stator cavity, intensification, turbulence intensity

Introduction

An important limitation for increasing chemical production rates per volume of reactor (i.e., intensification of the process) is the ability of the reactor to remove the produced heat of reaction. An inhomogeneous temperature distribution often results in decreasing reaction selectivity due to formation of by-products, and for highly exothermal reactions it can even lead to thermal runaway and overheating of the reactor surface.[1–4] Therefore, there is great interest in increasing the convective heat-transfer rate of chemical reactors, which is mainly done by application of passively enhanced heat exchangers for chemical conversion processes.[4–9] Well established passive heat-transfer enhancement techniques include plate heat exchangers[10,11] and plate fin heat exchangers.[12,13] One of the main difficulties in applying intensified heat exchangers as chemical reactors is the direct correlation between throughflow velocity and the convective heat-transfer rate. The residence time required for a reaction can be increased by either increasing the reactor length (resulting in a higher pressure drop) or by decreasing the throughflow velocity (resulting in a lower heat-transfer rate), for which thus an optimum must be found.[11,12,14,15] Active heat-transfer intensification of chemical reactors, which aims to enhance convective heat-transfer independently of throughflow velocity, has received little attention beyond classic stirred tank reactors.[16,17]

Correspondence concerning this article should be addressed to J. van der Schaaf at J.Vanderschaaf@tue.nl.

The rotor–stator spinning disc technology aims at increasing volumetric production rates by utilization of centrifugal forces and high-shear conditions. The technology is based on two closely spaced (typically 1–10 mm) parallel discs, rotating at different angular velocities (in case $\omega > 0$ rad s^{-1} the disc is called a rotor, when $\omega = 0$ rad s^{-1} the disc is called a stator), with the reaction fluid flowing through the axial gap between both discs. Due to the high velocity gradient a large shear force is exerted on the fluid, resulting in high turbulence intensities and large interfacial areas in the case of multiphase flows. This results in high volumetric rates of gas–liquid,[18] liquid–liquid,[19] and liquid–solid[20] mass-transfer in the rotor stator spinning disc reactor (rs-SDR). Fluid-stator heat-transfer coefficients have been shown to increase with increasing angular velocity as well,[17] up to h_s=8.8 kWm^{-2}K^{-1} at $\omega = 30$ rad s^{-1}. Moreover, h_s is shown to be independent of volumetric throughflow rate for $\omega > 5$ rad s^{-1}. The heat-transfer rate is then determined by the angular velocity of the rotor. The spinning disc technology is therefore a promising way to intensify heat and mass-transfer rates, independent of the residence time in the reactor. However, the overall heat-transfer performance of the rs-SDR (where the fluid inside the rotor–stator cavity was cooled using channels embedded in the stator wall) was rather limited, due to heat-transfer resistances presented by conduction through the stator wall and convection in the stator channels.[17]

The stator–rotor–stator spinning disc reactor (srs-SDR) aims to further increase the convective heat-transfer rates for chemical reactions, by enabling heat-transfer between two separate rotor–stator cavities. A single stator–rotor–stator stage consists of a stationary disc (inner stator) attached to a

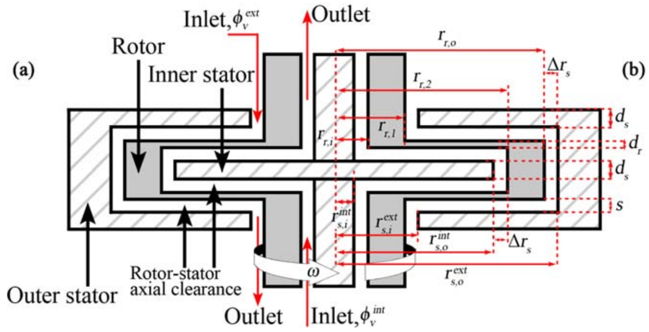

Figure 1. Schematic representation of a single stator–rotor–stator cavity.

It consists of a stationary disc (inner stator) enclosed by a rotating cylindrical housing (rotor), as shown in (a). The rotor is again enclosed by a stationary cylindrical housing (outer stator). In this way two rotor–stator cavities are obtained, separated by the common rotor. The axial gap between the rotor and the stators is low, typically in the range of millimeters. Nomenclature of the relevant dimensions used in this work are shown in (b). [Color figure can be viewed in the online issue, which is available at wileyonlinelibrary.com.]

central shaft, enclosed by a rotating cylindrical housing (rotor), see Figure 1. The rotor is again enclosed by a stationary cylindrical housing (outer stator). The axial clearance between the rotors and stators is low (2 mm). In this way, two rotor–stator cavities are obtained, separated by a common rotor. This common rotor acts as heat exchanging area, with fluid-rotor convective heat-transfer on both sides. The srs-SDR thus exerts high shear forces on both heat exchanging fluids, increasing convective transport of heat in both rotor–stator cavities.

The current work presents the novel stator–rotor–stator spinning disc reactor and its heat-transfer performance for single phase flow. Fluid-rotor heat-transfer coefficients are determined as a function of angular velocity and volumetric throughflow rate. The resulting heat-transfer coefficients are compared to results for rotor–stator systems available in literature. Additionally, the energy dissipation rate and the pressure drop (i.e., the energetic costs of the increased heat-transfer rates) are described. The (overall) thermal performance of the srs-SDR is compared with reactors commonly used in industry as well as with passively intensified reactor-heat exchanger concepts.

The steady-state heat-transfer model used to obtain the experimental heat-transfer coefficients is described in the Modeling Approach. The Experimental Section describes the experimental setup and procedure. In the Results and Discussion, the experimentally obtained heat-transfer coefficients are presented, followed by the rotational energy dissipation rate and the pressure drop over the reactor. Subsequently, the effectiveness of heat exchange in the srs-SDR is discussed. An evaluation of the srs-SDR and a comparison with other types of reactors is made in the Reactor Evaluation and Comparison, followed by the Conclusion.

Modeling Approach

A steady-state heat-transfer model is used to describe the fluid flow and heat-transfer in the srs-SDR. Experimentally obtained outlet temperatures are fitted with non-linear least square regression (MATLAB®) to this model, with the fluid-rotor heat-transfer coefficient h_r as fitting parameter. In the current work, the heat-transfer model presented by De Beer et al.[17] for a rs-SDR is applied to the srs-SDR. First, the fluid flow model is briefly described, followed by the applied heat-transfer model.

Fluid flow model

The fluid flow inside a rotor–stator cavity is modeled as regions of radial plug flow at low radial positions in combination with a single ideally mixed region at high radial positions.[21] This is a simplification of the hydrodynamics within rotor–stator cavities with externally applied throughflow. The plug flow at low radial positions represents a throughflow-dominated regime, where the radial velocity is centrifugal or centripetal over the entire rotor–stator axial gap (depending on the direction of the imposed throughflow). The ideally mixed region at high radial positions describes the rotation-dominated regime, where the radial velocity is centrifugal along the rotor and centripetal along the stator. Details of this fluid flow model can be found in De Beer et al.[21] Transition between the plug flow and ideally mixed regions is assumed to occur at a discrete radial position, r_{trans}. For fluid flow in the exterior cavity the relevant dimension* is $r_{\text{r,o}}$ and $r_{\text{trans}}^{\text{ext}}$ is determined from[17,21]:

$$\frac{r_{\text{trans}}^{\text{ext}}}{r_{\text{r,o}}}=\left(\frac{1}{c}\frac{C_w^{\text{ext}}}{\left(\text{Re}_\omega^{\text{ext}}\right)^{4/5}}\right)^{\frac{5}{13}} \tag{1}$$

For the interior cavity the relevant dimension is $r_{\text{s,o}}^{\text{int}}$ and $r_{\text{trans}}^{\text{int}}$ is determined from[17,21]:

$$\frac{r_{\text{trans}}^{\text{int}}}{r_{\text{s,o}}^{\text{int}}}=\left(\frac{1}{c}\frac{C_w^{\text{int}}}{\left(\text{Re}_\omega^{\text{int}}\right)^{4/5}}\right)^{\frac{5}{13}} \tag{2}$$

The proportionality constant c of Eqs. 1 and 2 is defined as[17,21]:

$$c=8.4\cdot 10^{-4}e^{146.6G} \qquad G<0.038 \tag{3}$$

$$c=0.219 \qquad G\geq 0.038 \tag{4}$$

where $G=G^{\text{ext}}$ for Eq. 1 and $G=G^{\text{int}}$ for Eq. 2, respectively.

The regions of radial plug flow in the exterior and interior cavities are modeled as forty continuous stirred tank reactors in series, as annular cylinders with evenly distributed volumes from $r_{\text{r,1}}$ to $r_{\text{trans}}^{\text{ext}}$ and from $r_{\text{s,i}}^{\text{int}}$ to $r_{\text{trans}}^{\text{int}}$, respectively. The well-stirred regions at high radial positions are modeled as single ideally stirred tanks.

Heat-transfer model

The heat-transfer model consists of enthalpy balances for each separate ideally stirred tank defined in the fluid flow model, see Figure 2. The enthalpy balance for each tank in the exterior cavity V_k is given by:

*In the current work dimensionless numbers are used to describe the fluid flow inside the rotor–stator cavities, as well as to compare the obtained heat-transfer coefficients with literature data. For the fluid flow the characteristic dimensions are $r_{\text{r,o}}$ for the exterior cavity and $r_{\text{s,o}}^{\text{int}}$ for the interior cavity. Dimensionless numbers pertaining to fluid flow in either of the cavities are indicated by the superscript ext and int, respectively. For heat-transfer the relevant dimension is $r_{\text{r,2}}$ as for $r>r_{\text{r,2}}$ the heat-transfer is negligible. A more accurate characteristic length would be obtained by integrating the local heat-transfer coefficient over the area relevant to heat-transfer, that is, $r_{\text{r,1}}$ to $r_{\text{s,2}}$ (e.g., 22,23). To perform this integration the radial dependency of the heat-transfer coefficient should be known, which is very sensitive to the applied boundary conditions.[17] Therefore, in the current work the characteristic length was chosen to be $r_{\text{r,2}}$. Dimensionless numbers relevant for heat-transfer have no superscript.

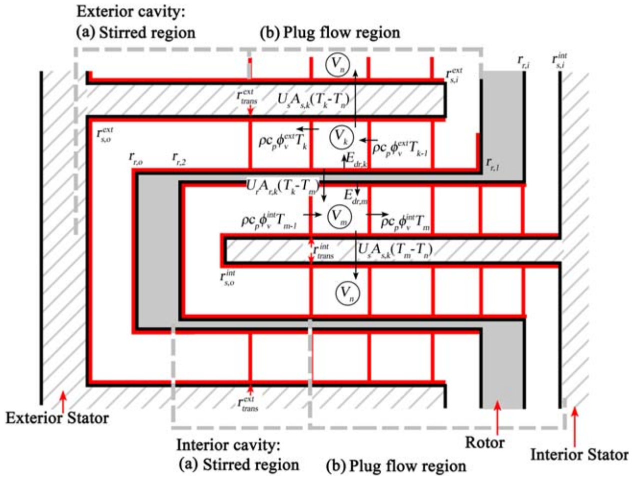

Figure 2. Schematic representation of the steady-state heat balances for each separate ideally stirred tank in the exterior cavity V_k and in the interior cavity V_m, as defined in the fluid flow model.

The plug flow regions at low radial positions are modeled as forty ideally stirred tank reactors in series, while the well-stirred region at high radial positions is modeled as a single ideally stirred tank. [Color figure can be viewed in the online issue, which is available at wileyonlinelibrary.com.]

$$\frac{d}{dt}(\rho V_k H_k) = \rho c_p \phi_v^{\text{ext}}(T_k - T_{k-1}) - U_r A_{r,k}(T_k - T_m) + \ldots \\ + U_s A_{s,k}(T_n - T_k) + E_{\text{dr},k} \\ = 0 \tag{5}$$

where V_{m} is the tank geometrically opposite of V_{k} on the other side of the rotor and V_{n} is the tank opposite of V_{k} on the other side of the stator. $E_{\text{dr,k}}$ is the energy dissipation rate for tank V_{k}. For each tank in the interior cavity V_m, the enthalpy balance is given by:

$$\frac{d}{dt}(\rho V_{\text{m}} H_{\text{m}}) = \rho c_p \phi_v^{\text{int}}(T_{\text{m}-1} - T_{\text{m}}) + U_{\text{r}} A_{\text{r},k}(T_k - T_{\text{m}}) + \ldots \\ - U_{\text{s}} A_{\text{s},m}(T_m - T_n) + E_{\text{dr},m} \\ = 0 \tag{6}$$

where V_k is the tank geometrically opposite of V_m on the other side of the rotor and V_n is the tank opposite of V_m on the other side of the stator. Steady-state is approached by solving Eqs. 5 and 6 for each tank for large t ($t/\tau_m > 1000$) using MATLAB® ODE15s solver routine.

The overall heat-transfer coefficient through the rotor U_{r} is defined according to:

$$U_{\text{r}} = \left(\frac{1}{h_{\text{r}}} + \frac{d_{\text{r}}}{k_{\text{w}}} + \frac{1}{h_{\text{r}}}\right)^{-1} \tag{7}$$

in which h_{r} is the actual fitting parameter. As no radially resolved temperature measurements are possible in the current setup, h_{r} for the plug flow and well-stirred regions can not be determined independently. Therefore, an equal value for h_{r} is assumed in both regions. The overall heat-transfer coefficient through the stator U_{s} is defined as:

$$U_{\text{s}} = \left(\frac{1}{h_{\text{s}}} + \frac{d_{\text{s}}}{k_{\text{w}}} + \frac{1}{h_{\text{s}}}\right)^{-1} \tag{8}$$

with: [17,24]

$$\frac{h_{\text{s}} r_{\text{r},2}}{k_{\text{f}}} = 0.0178 \text{Re}_{\omega}^{\frac{4}{5}} \left(\frac{\text{Pr}_{\text{water}}}{\text{Pr}_{\text{air}}}\right)^{\frac{3}{5}} \tag{9}$$

The rotor heat-transfer area of V_k and V_m is $A_{\text{r},k} = A_{\text{r},m} = \pi\left(r_{k+1}^2 - r_k^2\right)$, with $r_{\text{r},1} < r_k < r_{\text{r},2}$. The stator heat-transfer area of V_k and V_m is $A_{\text{s},k} = A_{\text{s},m} = \pi\left(r_{k+1}^2 - r_k^2\right)$, with $r_{\text{s,i}}^{\text{ext}} < r_k < r_{\text{s,o}}^{\text{ext}}$ for the exterior cavity and $r_{\text{s,i}}^{\text{int}} < r_k < r_{\text{s,o}}^{\text{int}}$ for the interior cavity.

The energy dissipation rate for V_k and V_m is determined by:

$$E_{\text{dr},j} = \int_{r_{j-1}}^{r_j} E_{\text{dr,loc}} r \, dr = \alpha r^2 r \, dr \qquad j = k, m \tag{10}$$

where the local energy dissipation rate $E_{\text{dr,loc}}$ is assumed to be proportional to the square of the local radius.[17,25] The proportionality constant α is obtained from experimental values of E_{dr}:

$$E_{\text{dr}} = 2\left(\int_{r_{\text{r,i}}}^{r_{\text{s,o}}^{\text{int}}} \alpha r^3 \, dr + \int_{r_{\text{s,i}}^{\text{ext}}}^{r_{\text{r,o}}} \alpha r^3 \, dr\right) \tag{11}$$

The rate of energy loss toward the environment and the rates of energy production due to liquid pressure drop over the interior and exterior cavities are neglected in the model, as discussed in the Experimental Section.

Experimental Section

Experimental setup

Figure 3 shows a schematic representation of the srs-SDR. The reactor (316L steel) consists of three stator–rotor–stator stages and a rotating conical gas–liquid separator. A single stator–rotor–stator stage exists of a stationary disc (the inner stator) attached to a central shaft, enclosed by a rotating cylindrical housing (the rotor) which is in turn again enclosed by a stationary cylindrical housing (the outer stator). The rotor is driven by a SEW Eurodrive CFM71M. The maximum angular velocity of 209 rad s^{-1} is determined by the applied dynamic lip seals of the reactor. Directly attached to the rotor is the gas–liquid separator, with separate outlets for both phases. As the scope of the current work was limited to a single liquid phase, the gas-liquid separator was not utilized and only a single outlet was used.

The outer radius of the rotor is $r_{\text{r,o}} = 71 \cdot 10^{-3}$ m. The axial gap between the rotor and both stators is $s = 2 \cdot 10^{-3}$ m, the radial gap is $\Delta r_{\text{s}} = 2 \cdot 10^{-3}$ m on both sides of the rotor. The reactor volume per stage is $V_R^{\text{int}} = 48.0 \cdot 10^{-6}$ m^3 for the interior rotor–stator cavity and $V_R^{\text{ext}} = 65.8 \cdot 10^{-6}$ m^3 for the exterior cavity. The rotor thickness is $d_{\text{r}} = 1 \cdot 10^{-3}$ m (between $r_{\text{r,1}} = 28 \cdot 10^{-3}$ m and $r_{\text{r,2}} = 60.5 \cdot 10^{-3}$ m), with a thermal conductivity[26] of $k_{\text{w}} = 16$ $\text{Wm}^{-1}\text{K}^{-1}$. The thickness of the rotor between $r_{\text{r},i}$ and $r_{\text{r,1}}$ and between $r_{\text{r,2}}$ to $r_{\text{r},o}$ is $10.5 \cdot 10^{-3}$ m. Therefore the effective heat-transfer area per stage is $A = 2\pi(r_{\text{r,2}}^2 - r_{\text{r,1}}^2) = 0.018$ m^2. The width of both the inner and outer stators is $d_{\text{s}} = 4 \cdot 10^{-3}$ m. The radius of the inner stator is $r_{\text{s,o}}^{\text{int}} = 58.5 \cdot 10^{-3}$ m.

Liquid (demineralized water) was fed to the top of the exterior cavity and withdrawn at the bottom. The liquid was

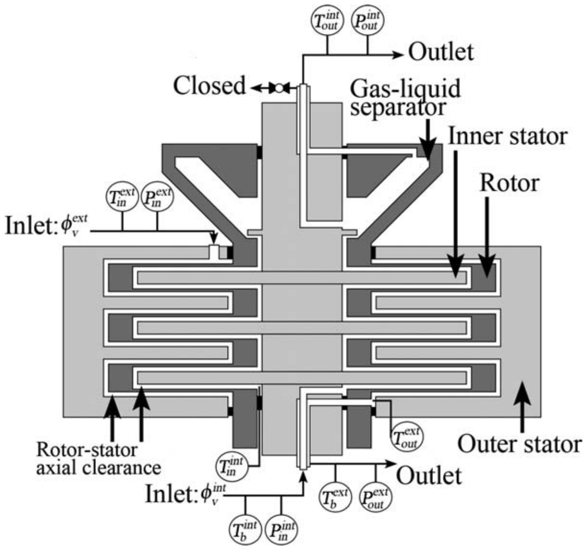

Figure 3. Schematic representation of the stator–rotor–stator spinning disc reactor.

The reactor consists of three separate stator–rotor–stator stages and a rotating conical gas–liquid separator. As the scope of the current work is limited to a single liquid phase, the gas–liquid separator is not used as such. The maximum angular velocity ω=209 rad s^{-1}. The outer rotor radius $r_{r,o}=71 \cdot 10^{-3}$ m. The axial clearance between the rotor and both stators $s=2 \cdot 10^{-3}$ m. Preheated liquid (water) is fed to the top of the exterior cavity and withdrawn at the bottom. Cooled liquid (water) is fed at the bottom of the interior cavity and withdrawn at the top. The heat exchanging liquids thus flow in countercurrent mode through the reactor. Fluid temperatures were measured at the inlet and outlets of both reactor cavities, as well as directly at the exit of the bottom exterior cavity. Gauge pressures were measured at the inlet and outlets of both cavities. The total current to the motor was monitored to determine the torque exerted on the rotor.

fed from a $10 \cdot 10^{-3}$ m^3 vessel, where it was preheated via internal coils (Lauda ECO RE 630, $\pm$0.02 K). The liquid volumetric flow rate was controlled by a Coriolis mass flow controller (Rheonik RHM 04), up to $\phi_v^{ext}=25 \cdot 10^{-6}$ m^{3}s^{-1}. Liquid (demineralized water) was fed at the bottom of the interior cavity and withdrawn at the top of the cavity; the liquid in the interior cavity flowed in countercurrent mode with respect to the liquid in the exterior cavity. The liquid was fed from a $10 \cdot 10^{-3}$ m^3 vessel, where it was cooled via internal coils (Lauda WKL4600, $\pm$0.5 K). The liquid volumetric flow rate was controlled by a Coriolis mass flow controller (Bronkhorst Cori-Flow M55), up to $\phi_v^{int}=25 \cdot 10^{-6}$ m^{3}s^{-1}. The reactor was completely enclosed by a stainless steel casing lined with double layers of HT/Armaflex insulation.

Fluid temperatures were measured using platinum resistive temperature detectors (PT100 1/10 DIN, $\pm$0.06°C). Temperatures were measured at the bottom and outlet of the interior cavity (T_b^{int} and T_{out}^{int}, respectively), the inlet and bottom of the exterior cavity (T_{in}^{ext} and T_b^{ext}, respectively), at the outlet of the exterior cavity (T_{out}^{ext}) and outside the reactor to monitor the temperature of the environment. To obtain T_{in}^{int} (the inlet temperature of the interior cavity) an enthalpy balance over the concentric tubes at the bottom of the reactor is used:

$$\begin{aligned}\frac{d}{dt}(\rho VH) &= \rho c_p \phi_v^{ext}\left(T_{out}^{ext}-T_b^{ext}\right)+\ldots \\ &\quad -\rho c_p \phi_v^{int}\left(T_{in}^{int}-T_b^{int}\right) \\ &= 0\end{aligned} \tag{12}$$

Gauge pressures were measured (Huba Control relative pressure transmitter type 520, $\pm$600 Pa) at the inlet and outlets of both the interior and exterior rotor–stator cavities. The pressure difference over the interior and exterior cavities was corrected for the hydrostatic pressure ($\rho g \Delta x^{int}=-5.3 \cdot 10^3$ Pa, $\rho g \Delta x^{ext}=4.1 \cdot 10^3$ Pa).

Heat-transfer measurements

Heat-transfer rates, Q_T, were determined from overall steady-state enthalpy balances over both the interior and exterior cavities of the srs-SDR. The volumetric flow rate on the exterior cavity side was $\phi_v^{ext}=15 \cdot 10^{-6}$ and $20 \cdot 10^{-6}$ m^{3}s^{-1} ($\pm 0.08 \cdot 10^{-6}$ m^{3}s^{-1}), corresponding to superposed dimensionless throughflow rates of $C_w^{ext}=211$ and 280, respectively. The exterior side inlet temperature T_{in}^{ext} ranged between 40 and 42.5°C. The volumetric flow rate on the interior cavity side was $\phi_v^{int}=15 \cdot 10^{-6}$ and $20 \cdot 10^{-6}$ m^{3}s^{-1} ($\pm 0.08 \cdot 10^{-6}$ m^{3}s^{-1}), corresponding to $C_w^{int}=256$ and 341, respectively. The interior side feed temperature T_b^{int} ranged from 23 to 25°C. The angular velocity ω ranged between 0 and 157 rad s^{-1} ($\pm$0.05 rad s^{-1}), corresponding to rotational Reynolds numbers of $Re_\omega^{ext}=0$ to $7.9 \cdot 10^5$ ($Re_\omega^{int}=0$ to $5.4 \cdot 10^5$). The axial clearance between the rotor and the stators was kept constant at $s=2 \cdot 10^{-3}$ m for both the exterior and the interior cavities, corresponding to gap ratios of $G^{ext}=0.028$ and $G^{int}=0.034$, respectively. The heat-transfer rates ranged from Q_T = 240–850 W.

The overall steady-state enthalpy balance is shown in Eq. 13, including the contributions of heat production due to pressure drop on both the exterior and interior sides, the heat loss to the environment and the heat produced due to the rotational motion of the rotor.

$$\begin{aligned}\frac{d}{dt}(\rho VH) &= \rho c_p \phi_v^{ext}\left(T_{in}^{ext}-T_{out}^{ext}\right)+\ldots \\ &\quad -\rho c_p \phi_v^{int}\left(T_{out}^{int}-T_{in}^{int}\right)+\ldots \\ &\quad +E_{dp}^{ext}+E_{dp}^{int}-E_{loss}+3E_{dr} \\ &= 0\end{aligned} \tag{13}$$

Equation 13 was closed normally distributed within 4% of Q_T for $\omega \geq 10$ rad s^{-1}. For $\omega \leq 5$ rad s^{-1} the deviation is at maximum 16% of Q_T. This is possibly due to tangential maldistribution at low angular velocities, which results in erroneous temperature measurements of T_{out}^{ext}, as this temperature sensor is located at a single tangential position at the exit of the exterior cavity. This is supported by the fact that the deviation is largest for $\omega = 0$ rad s^{-1}.

The rate of energy production due to pressure drop[27] ($E_{dp}=\phi_v \Delta P$) was at maximum 0.55 W (at $C_w^{ext}=280$ and $Re_\omega^{ext}=5.3 \cdot 10^5$), which is 0.23% of the lowest Q_T. The rate of energy loss to the environment was obtained by keeping $T_{in}^{ext}=T_b^{int}=45^\circ$C, $\omega = 0$ rad s^{-1} and measuring T_b^{ext} and T_{out}^{int}. The value of E_{loss} is obtained by:

$$E_{\mathrm{loss}}=\rho c_p \phi_{\mathrm{v}}^{\mathrm{ext}}\left(T_{\mathrm{in}}^{\mathrm{ext}}-T_b^{\mathrm{ext}}\right)+\rho c_p \phi_{\mathrm{v}}^{\mathrm{int}}\left(T_b^{\mathrm{int}}-T_{\mathrm{out}}^{\mathrm{int}}\right)+E_{dp}^{\mathrm{ext}}+E_{dp}^{\mathrm{int}}=0 \quad (14)$$

The value of E_{loss} was maximum 9 W, which is 3.8% of the lowest Q_T.

The rotational energy dissipation rate per stage was calculated using the torque exerted on the rotor, Eq. 15.

$$E_{\mathrm{dr}}=\frac{\omega\tau}{3}=\frac{\omega(I-I_0)\tau_c I_c}{3} \quad (15)$$

Values of τ were obtained by measuring the current I supplied to the motor, from which the internal current losses of the motor I_0 were subtracted, and multiplying it by motor characteristics τ_c=0.98 NmA^{-1} and $I_c=4$ A. It should be noted that the values of E_{dr} are corrected for the idle energy uptake of the motor, but not for the idle energy uptake of the reactor (e.g., due to dynamic seals), which strictly make E_{dr} specific for the current setup. However, as the overall enthalpy balance was closed within 4% of Q_T, it was concluded that the values of E_{dr} are close to the energy actually dissipated into the liquid. The rotational dissipation rate is maximum 160 W at $\mathrm{Re}_\omega^{\mathrm{ext}}=7.9\cdot 10^5$ which is maximum 30% of Q_T.

The effectiveness of heat exchange η was determined from Eq. 16, defined on the high-temperature stream $\phi_{\mathrm{v}}^{\mathrm{ext}}$:

$$\eta=\frac{Q_T}{Q_{\mathrm{max}}}=\frac{\rho c_p \phi_{\mathrm{v}}^{\mathrm{ext}}\left(T_{\mathrm{in}}^{\mathrm{ext}}-T_{\mathrm{out}}^{\mathrm{ext}}\right)}{\rho c_p \phi_{\mathrm{v}}^{\mathrm{ext}}\left(T_{\mathrm{in}}^{\mathrm{ext}}-T_{\mathrm{in}}^{\mathrm{int}}\right)} \quad (16)$$

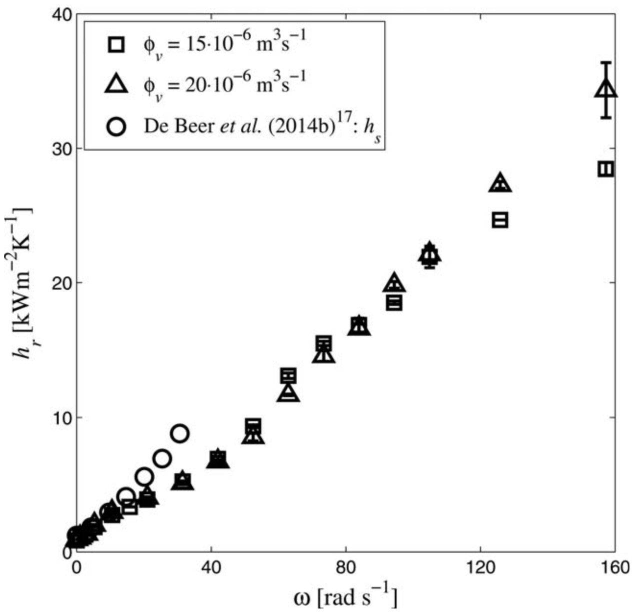

Figure 4. Experimentally obtained values of h_r as function of ω for ϕ_v=15 · 10^{-6} (□) and ϕ_v=20 · 10^{-6} m^{3}s^{-1} (△) and values for h_s obtained by De Beer et al.[17] (○).

The values of h_r are independent of ϕ_v and increase with increasing ω, up to h_r = 34 kWm^{-2}K^{-1} at ω = 157 rad s^{-1}. This is in accordance with the rotation dominated heat-transfer regime observed in literature.[28] For ω>15 rad s^{-1}, h_s is up to 80% larger than h_r.

Results and Discussion

Fluid–rotor heat-transfer

The values for the fluid–rotor heat-transfer coefficients are obtained by fitting the experimental steady-state outlet temperatures (on both exterior and interior cavity sides) to the steady-state heat-transfer model described in the Modeling Approach. The resulting values are depicted in Figure 4 as a function of ω for $\phi_{\mathrm{v}}^{\mathrm{ext}}=\phi_{\mathrm{v}}^{\mathrm{int}}=15\cdot10^{-6}$ (□) and $20\cdot10^{-6}$ m^{3}s^{-1} (△). The values of h_{r} increase with increasing angular velocity and are independent of volumetric throughflow rate. This is in accordance with the rotation dominated heat-transfer regime observed in literature,[17,28,29] where heat-transfer rates are independent of volumetric throughflow rate and rotor–stator distance. The maximum value of h_{r} is 34 kWm^{-2}K^{-1} at $\omega=157$ rad s^{-1} and $\phi_{\mathrm{v}}=20\cdot10^{-6}$ m^{3}s^{-1}. Figure 4 also displays the fluid–stator heat-transfer coefficients, h_{s} (○), obtained in the multistage rotor–stator spinning disc reactor.[17] The values of h_{r} are qualitatively similar to the values of h_{s}, however for $\omega>15$ rad s^{-1}, h_{s} is up to 80% higher than h_{r}. This difference is discussed further below. As h_{r} increases, U_{r} increases with increasing ω as well. A maximum value of 8.3 kWm^{-2}K^{-1} is obtained at $\omega=157$ rad s^{-1} and $\phi_{\mathrm{v}}=20\cdot10^{-6}$ m^{3}s^{-1}. For $\omega>120$ rad s^{-1}, U_{r} is mainly limited by conduction through the rotor $d_{\mathrm{r}}k_{\mathrm{w}}^{-1}$.

Figure 5 shows the dimensionless fluid–rotor heat-transfer coefficient Nu_{r}, as a function of Re_ω for $\phi_{\mathrm{v}}=15\cdot10^{-6}$ (□) and $20\cdot10^{-6}$ m^{3}s^{-1} (△). For $\mathrm{Re}_\omega<1.1\cdot10^5$ a laminar regime is observed, which is described by Eq. 17 (- -, in Figure 5). The observed $\mathrm{Nu}_r^{\mathrm{lam}}\propto\mathrm{Re}_\omega^{1/2}$ is in accordance with literature.[24,32–34] Equation 17 is, after correcting for water as a fluid with[34] $(\mathrm{Pr}_{\mathrm{air}}/\mathrm{Pr}_{\mathrm{water}})^{1/2}$, 23% higher than the laminar correlation for a free[†] disc[33] and 35% lower than for laminar flow in an enclosed[†] disc.[24] Given the uncertainty associated with the fluid correction factor of $\mathrm{Pr}^{1/2}$ (no experimental validation is present in literature), this is relatively close.

For $\mathrm{Re}_\omega>2.3\cdot10^5$ a turbulent regime is observed, described by Eq. 19 (- ·, in Figure 5). The observed $\mathrm{Nu}_r^{\mathrm{turb}}\propto\mathrm{Re}_\omega^{4/5}$ is in accordance with literature.[24,33–35] Eq. 19 is, with a correction of[34] $(\mathrm{Pr}_{\mathrm{air}}/\mathrm{Pr}_{\mathrm{water}})^{3/5}$, 22% lower than the turbulent correlation for a free disc[35] and 15% lower than for turbulent flow in an enclosed disc.[24] Again, for the fluid correction factor of $\mathrm{Pr}^{3/5}$ no experimental validation is present, hence Eq. 19 is in relatively good agreement with literature.

In between these two extremes, for $1.1\cdot10^5<\mathrm{Re}_\omega<2.3\cdot10^5$, a transition from laminar to turbulent flow occurs. This appears to be in agreement with literature, where the onset of transition from laminar to turbulent flow is usually observed at $\mathrm{Re}_\omega=0.8-1.5\cdot10^5$ for rotor–stator systems without externally applied throughflow.[25,34,36,37‡] Quantative information on the dependency of Re_ω on Nu_{r} in the transitional regime of rotating systems is scarce. For the free disc usually $\mathrm{Nu}_{\mathrm{r}}^{\mathrm{trans}}\propto\mathrm{Re}_\omega^2-\mathrm{Re}_\omega^4$ is observed.[38–40] For an enclosed disc $\mathrm{Nu}_{\mathrm{r}}^{\mathrm{trans}}\propto\mathrm{Re}_\omega^{1.06}$ is reported,[41] while for liquid–rotor mass transfer in a rs-SDR a dependency of Re_ω^2 is reported.[20] The values of $\mathrm{Nu}_{\mathrm{r}}^{\mathrm{trans}}$ in the current work are found

[†] A free disc is a single rotor rotating in a quiescent environment, an enclosed disc consists of a rotor fully enclosed by a cylindrical stator. In both systems no external throughflow is applied.

[‡] For rotor–stator systems with externally applied throughflow, no quantitative data on the values of Re_ω for which the laminar-turbulent transition occurs is available.

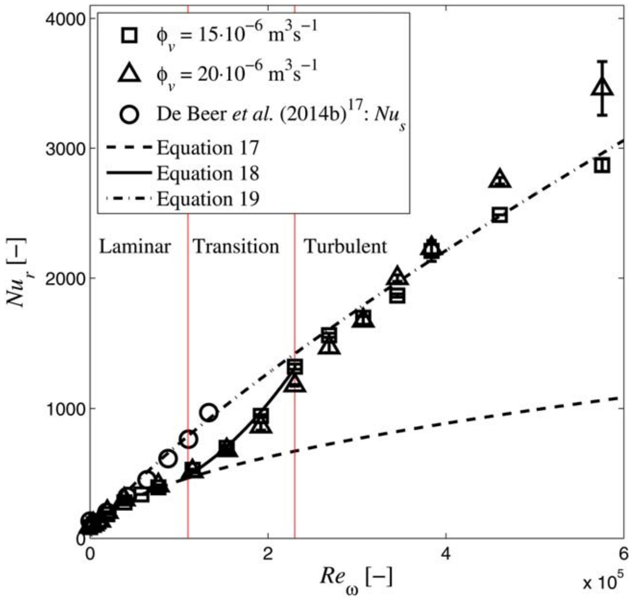

Figure 5. Experimentally obtained values of Nu_r are shown as function of Re_ω for $\phi_v=15\cdot10^{-6}$ (□) and $\phi_v=20\cdot10^{-6}$ m^3s^{-1} (△), as well as values for Nu_s obtained by De Beer et al.[17] (○).

For $Re_\omega<1.1\cdot10^5$, a laminar regime is observed, described by Eq. 17 (- -), while a turbulent regime is observed for $Re_\omega>2.3\cdot10^5$, described by Eq. 19 (- ·). The transition between both regimes for $1.1\cdot10^5<Re_\omega<2.3\cdot10^5$, is described by Eq. 18 (—). Transition from laminar to turbulent occurs at lower Re_ω for Nu_s than for Nu_r, which is in agreement with literature.[30,31][Color figure can be viewed in the online issue, which is available at wileyonlinelibrary.com.]

to be described by Eq. 18 (—, in Figure 5). The observed $Nu_r^{trans}\propto Re_\omega^{2.14}$ is similar to the liquid–rotor mass-transfer correlation presented by Meeuwse et al.[20]

$$Nu_r^{lam}=1.4\ Re_\omega^{\frac{1}{2}} \qquad Re_\omega<1.1\cdot10^5 \quad (17)$$

$$Nu_r^{trans}=3.5\cdot10^{-9}\ Re_\omega^{2.14}+267 \qquad 1.1\cdot10^5\le Re_\omega<2.3\cdot10^5 \quad (18)$$

$$Nu_r^{turb}=0.073\ Re_\omega^{\frac{4}{5}} \qquad Re_\omega\ge2.3\cdot10^5 \quad (19)$$

Comparing the values of Nu_r to the values of Nu_s[17] (○ in Figure 5), it can be seen that in the current work turbulence is obtained at much higher values of Re_ω. For $Re_\omega<0.4\cdot10^5$ the values of Nu_r are equal to the values of Nu_s, but Nu_r reaches the turbulent level only for $Re_\omega\ge2.3\cdot10^5$. The values of Nu_s are at a turbulent level already for $Re_\omega>0.4\cdot10^5$. Qualitatively, this is in accordance with literature, where turbulence is observed at lower Reynolds numbers at the stator then at the rotor.[30,31,36] This is argued to be due to the fluid in the rotor boundary layer being fed from the laminar region close to the shaft (as along the rotor the radial velocity is centrifugal), while the fluid in the stator boundary layer is being fed from the turbulent region at the rim of the rotor (as along the stator the radial velocity is centripetal).[31]

For engineering purposes it is clear that single phase heat-transfer in spinning disc reactors (both rotor–stator and stator-rotor–stator SDR) is well predicted by Eqs. 17 and 19. For fluid–rotor heat-transfer both the laminar and turbulent flow regimes need to be considered, while for fluid–stator heat-transfer the correlation for Nu_s for turbulent flow is sufficient in practice.[17]

Rotational energy dissipation rate

Figure 6 displays the values of E_{dr} per stator–rotor–stator stage (obtained by Eq. 15) as a function of Re_ω^{ext} for $\phi_v^{ext}=\phi_v^{int}=15\cdot10^{-6}$ (□) and $20\cdot10^{-6}$ m^3s^{-1} (△). The value of E_{dr} increases with increasing Re_ω^{ext} and is independent of ϕ_v, which is in accordance with literature.[17,25,42] The empirical correlation for the rate of rotational energy dissipation in a rotor–stator spinning disc reactor presented by De Beer et al.,[17] Eq. 20, is shown in Figure 6 (—).

$$E_{dr}=2\cdot\left(5.73\cdot10^{-12}(G^{ext})^{-0.14}\left(Re_\omega^{ext}\right)^{2.12}\right) \quad Re_\omega^{ext}<11\cdot10^5 \tag{20}$$

The original correlation[17] is presented for a single rotor–stator stage (i.e., for two rotor–fluid interfaces); because a stator-rotor–stator stage consists of four rotor–fluid interfaces (see Figure 1) the correlation is multiplied by two for each stator–rotor–stator stage, yielding Eq. 20. Figure 6 shows that for $Re_\omega^{ext}\ge1.5\cdot10^5$ the current values of E_{dr} are well described by Eq. 20, deviations are within 5%. For $Re_\omega^{ext}<1.5\cdot10^5$ larger deviations are observed. This is possibly explained by friction due to the dynamic lip seals: with increasing angular velocity a lubricating liquid film forms between the seal and the shaft, decreasing the friction resistance.[43,44] The observation that for $Re_\omega^{ext}\ge1.5\cdot10^5$ the values of E_{dr} are well described by Eq. 20 (which was obtained using an overall enthalpy balance for a rs-SDR[17]), indicates that E_{dr} is indeed close to the rates of energy actually dissipated into the liquid (see the Experimental Section). The correlation presented by Daily and Nece[25] for the rate of energy dissipation in an enclosed disc (for turbulent flow and small rotor–stator axial gap), is shown in Figure 6 (- -). In the rs-SDR $E_{dr}\propto\left(Re_\omega^{ext}\right)^{2.12}$, whereas for the enclosed disc $E_{dr}\propto\left(Re_\omega^{ext}\right)^{\frac{11}{4}}$. This difference is possibly explained by the relatively low values of Re_ω^{ext} for which Eq. 20 was obtained: $Re_\omega^{ext}\le11\cdot10^5$ for the rs-SDR,[17] compared to $Re_\omega^{ext}=10^7$ for the enclosed disc.[25]

Pressure drop

The total pressure drop over the srs-SDR for the exterior and interior cavities is shown in Figure 7 as a function of Re_ω^{ext} and C_w^{ext} and Re_ω^{int} and C_w^{int}, respectively. Both ΔP_T^{int} and ΔP_T^{ext} increase with increasing $Re_\omega^{ext/int}$ and increasing $C_w^{ext/int}$, which is qualitatively consistent with pressure measurements in literature.[45–47] For ΔP_T^{ext} this increase with Re_ω^{ext} and C_w^{ext} is linear, as was observed for the rs-SDR.[17] For ΔP_T^{int} a linear increase with Re_ω^{int} is observed at higher values of Re_ω. The different offset for ΔP_T^{ext} and ΔP_T^{int} at $Re_\omega^{ext/int}=0$ is not fully understood, however at high angular velocities ΔP_T^{ext} and ΔP_T^{int} appear to be similar. The values of ΔP_T include, apart from the pressure drop over the stator–rotor–stator stages, the internal inlet and outlet tubes with sharp 90° bends. It is estimated[§] that 20–50% of the total pressure drop is due to these inlet and outlet tubes.

[§]A correction for the inlet and outlet tubes and sharp bends inside the reactor (to yield a net pressure drop over the stator–rotor–stator stages) was estimated by using the Darcy-Weisbach equation[27] with the correlation presented by Blasius[48] to estimate the f_F for straight tubes and assuming $f=1.3$ for each 90° bend.[49]

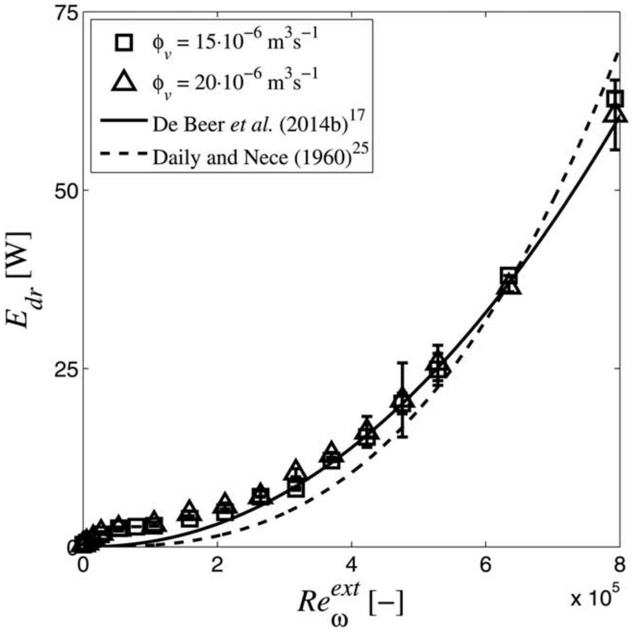

Figure 6. Experimentally obtained values of E_{dr} as function of Re_ω^{ext} for $\phi_v=15 \cdot 10^{-6}$ (□) and $\phi_v=20 \cdot 10^{-6}$ m^{3}s^{-1} (△).

The empirical correlation for E_{dr} in a rs-SDR presented by De Beer et al.,[17] Eq. 20, is shown (–-), as well as the correlation presented by Daily and Nece[25] for E_{dr} in an enclosed disc for turbulent flow and small rotor–stator axial clearance (- -). E_{dr} increases with increasing Re_ω^{ext} and is well described by Eq. 20. In the SDR $E_{dr} \propto (Re_\omega^{ext})^{2.12}$, whereas for the enclosed disc[25] $E_{dr} \propto (Re_\omega^{ext})^{\frac{11}{4}}$.

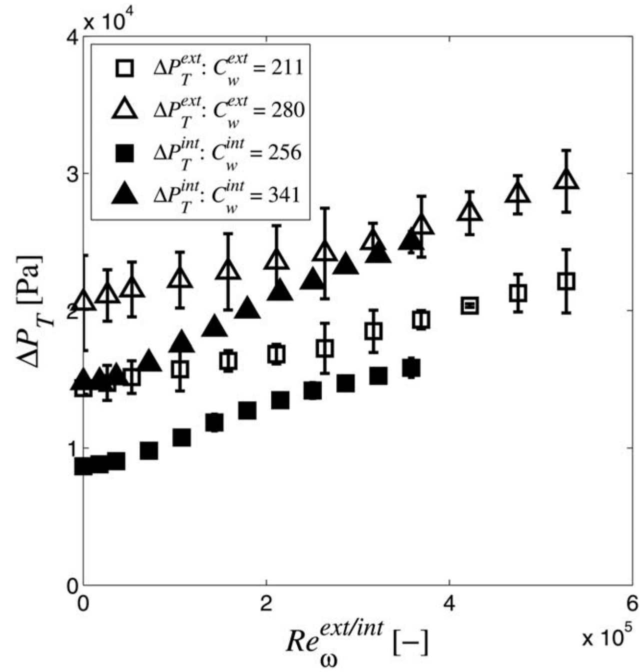

Figure 7. Experimentally obtained values of ΔP_T^{ext} as function of Re_ω^{ext} for $\phi_v^{ext}=15 \cdot 10^{-6}$ ($C_w^{ext}=211$, □) and $\phi_v^{ext}=20 \cdot 10^{-6}$ m^{3}s^{-1} ($C_w^{ext}=280$, △) and ΔP_T^{int} as function of Re_ω^{int} for $\phi_v^{int}=15 \cdot 10^{-6}$ ($C_w^{int}=256$, ■ $C_w^{int}=256$, ■) and $\phi_v^{int}=20 \cdot 10^{-6}$ m^{3}s^{-1} ($C_w^{int}=341$, ▲ $C_w^{int}=341$, ▲).

Both ΔP_T^{ext} and ΔP_T^{int} increase with increasing angular velocity and volumetric throughflow rate.

Heat exchange effectiveness

Figure 8 shows the effectiveness η of heat exchange in the srs-SDR (for three stages) as a function of angular velocity, for volumetric throughflow rates of $\phi_v^{ext}=\phi_v^{int}=15 \cdot 10^{-6}$ (□) and $20 \cdot 10^{-6}$ m^{3}s^{-1} (△). The values of η increase from 0.24 to 0.61 by increasing ω from 0 to 83 rad s^{-1}, for $\phi_v=20 \cdot 10^{-6}$ m^{3}s^{-1}. This is explained by the increasing U_r with increasing ω, as for any heat exchanger η is a positive function of $(UA/\rho c_p \phi_v)$.¶ This explains as well why η decreases with increasing ϕ_v and constant ω: a higher thermal load $(\rho c_p \phi_v)$ requires a higher capacity heat exchanger.

For $\omega > 83$ rad s^{-1}, η decreases with increasing ω, whereas a further increase of U_r is observed. This is due to the rotational energy dissipation rate being no longer negligible compared to Q_T; instead of approaching T_{in}^{int} further, T_{out}^{ext} increases with increasing ω. Therefore, the effectiveness of the srs-SDR as a heat exchanger can not be increased indefinitely by increasing ω alone; the heat exchanging area needs to be increased by increasing the number of stages. Obviously, when the aim of the heat exchanger is to heat up a stream (and not necessarily to cool down the other) this limitation is not relevant.

Reactor Evaluation and Comparison

Convective heat-transfer coefficients

Convective heat-transfer rates are increased by increasing the specific energy rate ϵ dissipated into the fluid. Figure 9 displays the currently obtained values of h_r (□) as a function of $\epsilon=(E_{dr}+\Delta P \phi_v)V_L^{-1}$. The transition from laminar to turbulent can be clearly noticed by the steep increase of h_r for $\epsilon > 10^5$ Wm$_L^{-3}$. The observed trends of $h_r=f(\epsilon)$ are in agreement with rotor–stator systems described in literature: for the laminar regime $h_r \propto \epsilon^{\frac{1}{4}}$ (from[25] $\epsilon \propto \omega^2$ and[32] $h_r \propto \omega^{\frac{1}{2}}$), for the turbulent regime $h_r \propto \epsilon^{0.29}$ (from[25] $\epsilon \propto \omega^{\frac{11}{4}}$ and[32] $h_r \propto \omega^{\frac{4}{5}}$).

Figure 9 also displays correlations for the heat-transfer coefficients in tubular reactors (solid line for $d_h=10 \cdot 10^{-3}$ m), plate heat exchangers (dashed line for $d_h=2 \cdot 1.5 \cdot 10^{-3}$ m) and plate fin heat exchangers (circular markers with solid line, $d_h=2 \cdot 10^{-3}$ m), for comparison. The equations used in Figure 9 can be found in Appendix A. The correlations for laminar and turbulent regimes are displayed by the thick lines, the transition between laminar to turbulent regimes is indicated by the thin lines. Practical operation limits for the considered reactor-heat exchangers are indicated in Figure 9 as shaded boxes.** From the correlations displayed in Figure 9 it can be observed that the correlation between ϵ and h is rather similar for all turbulent flows considered: $h \propto \epsilon^{0.24} - \epsilon^{0.29}$. This is close to $h \propto \epsilon^{\frac{1}{4}}$ observed by

¶$\eta=f(\rho c_p \phi_v^{ext}/\rho c_p \phi_v^{int})$ is not considered in the current work as $\phi_v^{ext}=\phi_v^{int}$ for all measurements.

**The upper practical limit of ϵ for tubular, plate and plate fin reactor-heat exchangers is assumed to be $\Delta P \tau_m^{-1} = 1 \cdot 10^5$ Pa per second residence time, a typical operating value for passively enhanced heat exchangers.[10,11,14] Obviously, this limit is rather arbitrary: at the expense of a higher pressure drop, operation at higher values of ϵ is possible. The lower practical limit of ϵ for tubular reactors is the point where transition from the turbulent to the laminar regime starts, before which h rapidly decreases. This rapid decrease of h with decreasing ϵ does not occur for plate and plate fin heat exchangers, therefore no lower practical limit of ϵ for the compact heat exchangers is indicated.

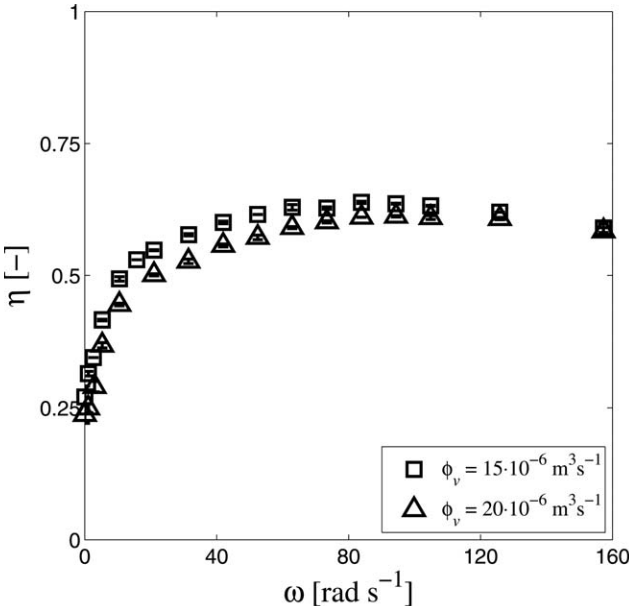

Figure 8. Effectiveness of heat exchange η as function of ω, for $\phi_v = 15 \cdot 10^{-6}$ (□) and $\phi_v = 20 \cdot 10^{-6}$ m^3s^{-1} (△).

The values of η increase with increasing ω, indicating that (without application of any model) U_r increases with increasing ω. For ω>83 rad s^{-1}, η decreases with increasing ω due to E_{dr} being no longer negligible compared to Q_T; T_{out}^{ext} increases, instead of approaching T_{in}^{int}.

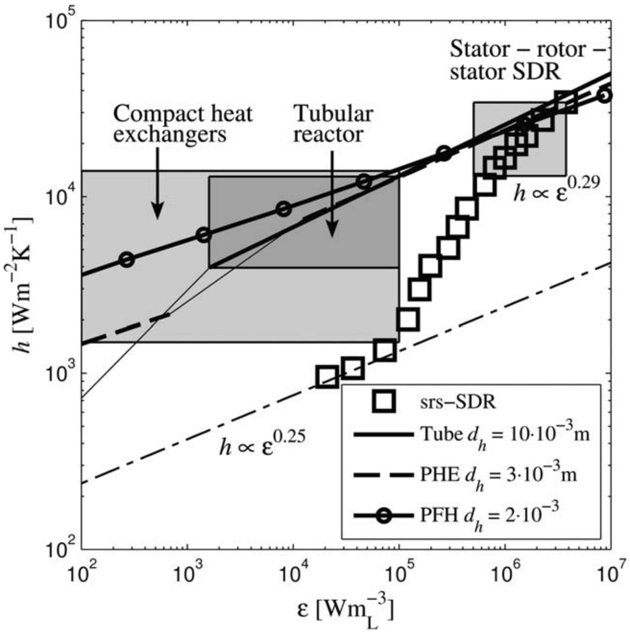

Figure 9. Experimentally obtained values of h_r as function of ϵ for $\phi_v = 15 \cdot 10^{-6}$ (□).

For the laminar regime $h_r \propto \epsilon^{\frac{1}{4}}$, for the turbulent regime $h_r \propto \epsilon^{0.29}$, which is in agreement with literature[25,34]). Correlations for the heat-transfer coefficients in tubular reactors (–-, for $d_h = 10 \cdot 10^{-3}$ m), plate heat exchangers (- -, PHE, for $d_h = 1.5 \cdot 10^{-3}$ m) and plate fin heat exchangers (solid line with circular marker, PFH, $d_h = 2 \cdot 10^{-3}$ m) are shown. Practical operation limits[A] for the considered reactor-heat exchangers are indicated as shaded boxes. The values of h_r obtained in the srs-SDR are a factor 2–3 higher than film coefficients practically achievable in established reactor-heat exchangers, due to the higher values of ϵ than can be realised in the spinning disc reactor.

Calderbank and Moo-Young,[50] who correlated this to the Kolmogorov length scale of the smallest eddies (which is proportional to[51] $\epsilon^{-\frac{1}{4}}$). Therefore it can be concluded that the convective heat-transfer coefficient is mainly determined by the turbulence intensity in the fluid, irrespective of it being induced in an active way (as is the case in the srs-SDR), or in a passive way by introducing a high pressure drop.[11] However, as the shaded boxes in Figure 9 indicate, the values of h_r obtained in the srs-SDR are a factor 2–3 higher than film coefficients practically achievable in established reactor-heat exchangers. This is due to the higher values of ϵ that can be realized in the spinning disc reactor, that is, the high levels of turbulence intensity allow intensification of the convective heat-transfer. For $\epsilon < 3 \cdot 10^5$ Wm_L^{-3} it is clear that the passive enhancement techniques perform much better than the srs-SDR, due to the rather steep decline in h_r observed in the srs-SDR at the transition from turbulent to laminar flow regime. Preventing this steep decline in h at low values of ϵ is indeed the main aim of passive heat-transfer enhancement.[14]

Reactor operation

As was discussed previously, the convective heat-transfer coefficient in turbulent flow is mainly determined by intensity of turbulence dissipation into the fluid. In the srs-SDR specific energy dissipation rates up to $\epsilon = 3.9 \cdot 10^6$ Wm_L^{-3} are achieved for $\omega = 157$ rad s^{-1}, yielding $h_r = 34$ $kWm^{-2}K^{-1}$. The advantage of the current srs-SDR (compared to passive heat-transfer enhancement) is that the turbulence intensity can be easily increased by increasing the angular velocity of the rotor, whereas passive enhancement depends on pump capacity to increase ΔP. Moreover, the turbulence intensity in the current setup is increased independently of volumetric throughflow rate, and thus independently of residence time. As for passive heat-transfer enhancement[27] $\epsilon = \Delta P \phi_v V_L^{-1} = \Delta P \tau_m^{-1}$, achieving $\epsilon > 10^6$ for any $\tau_m > 1$ s yields prohibitively high pressure drops, for example, 100 $\cdot 10^5$ Pa for $\tau_m = 10$ s. As in the srs-SDR the turbulence intensity is independent of τ_m, intensification of the convective heat-transfer at high ϵ is possible for chemical reactions requiring $\tau_m > 1$ s.

At low ϵ (the main range of interest for passive heat-transfer enhancement), application of the srs-SDR is not justified however (see Figure 9). This is due to the relatively high values of E_{dr} for $Re_\omega < 1.5 \cdot 10^5$ and low laminar values of h_r.

It should be noted that although in the current range of operating conditions ($\phi_v = 15-20 \cdot 10^{-6}$ m^3s^{-1}, $\tau_m = 7-10$ s) the pressure drop over the total reactor is low (see Figure 7), ΔP increases linearly with increasing ϕ_v and increasing τ_m (i.e., number of stages). For scale-up of production capacity of the srs-SDR and/or long residence times, the pressure drop can get prohibitively high (similar to the limitations of the passive enhancement techniques). A possible solution is increasing the reactor dimensions r and $s = rG$, which increases ϕ_v at constant C_w or increases τ_m at constant ϕ_v. As $\epsilon \propto r^{-3}$ ($V_L \propto r^3 G$) and $\epsilon \propto Re_\omega^{2.12}$, ω has to increase with $r^{2.12/3}$ (and thus with $\phi_v^{2.12/3}$) to maintain ϵ. Therefore, at constant C_w and G, $\Delta P \propto \phi_v^{2.12/3}$ for a constant ϵ. This indicates that scale-up of production capacity is feasible by increasing reactor dimensions. However, as ΔP increases with increasing ϕ_v, a combination of dimensional scale-up and parallelization will be required for high values of ϕ_v.

Overall heat-transfer performance

The degree of heat-transfer intensification achievable in a chemical reactor is determined by UAV_R^{-1} rather than by the value of h alone. Due to the high values of h_r, the values of U_r obtained in the srs-SDR are relatively high as well (up to U_r=8.3 kWm^{-2}K^{-1}), compared to U=3−7 kWm^{-2}K^{-1} for plate heat exchangers and tubular reactors.[10,11,26,52] For plate reactors U=2−2.5 kWm^{-2}K^{-1} is typically obtained.[7] In the current setup it is observed that at high angular velocities ($\omega > 80$ rad s^{-1}), U_r is mainly determined by conduction through the rotor. Therefore, increasing U_r further can rather be achieved by decreasing the thickness of the rotor d_r and/or working with a higher thermal conductivity material (e.g., tantalum[26] $k = 57$ W m^{-1}K^{-1}, aluminium[26] $k = 237$ W m^{-1}K^{-1}, sintered silicon carbide[53] $k = 120$ W m^{-1}K^{-1}), than by increasing the angular velocity further. For example, using a rotor of $1 \cdot 10^{-3}$ m tantalum will yield U_r=13.1 kWm^{-2}K^{-1} at $\omega = 157$ rad s^{-1}. It is clear that with further (mechanical) optimization, the thermal performance of the srs-SDR can be greatly enhanced.

The specific heat-transfer area of the srs-SDR is, with AV_R^{-1}=375 m^{2}m^{-3}, rather low. For tubular reactors[52,54] AV_R^{-1}=80−400, while for plate heat exchangers[10,11] AV_R^{-1} =120−660 m^{2}m^{-3}. Partially this is due to constructional constraints of the prototype; only 58% of the total rotor area is used as effective heat-transfer area. Without this limitation AV_R^{-1}=647 m^{2}m^{-3}, making it comparable to values obtained in plate heat exchangers. The ratio of AV_R^{-1} can be further increased by either reducing the rotor–stator distance (which will lead to a higher ΔP), or by increasing the effective heat-transfer area using nonflat discs.

In the srs-SDR a maximum value of UAV_R^{-1}=3.1 MWm$_L^{-3}$K^{-1} (or 5.4 MWm$_L^{-3}$K^{-1} for AV_R^{-1}=647 m^{2}m^{-3}) is obtained at ϵ=3.9 MWm$_L^{-3}$. This is a factor 2–5 larger than what is achieved in tubular reactors and a factor 1.2–10 times higher than the UAV_R^{-1} of plate heat exchangers. However, ϵ is 1–2 orders of magnitude larger in the srs-SDR compared to the tubular and plate reactors-heat exchangers. It can therefore be concluded that although the current srs-SDR allows intensification of the convective heat-transfer, it comes at a relatively high energetic expense. It should be noted that as the values of h_r practically achievable in the srs-SDR are high compared to the alternatives (see the Reactor Evaluation and Comparison), it appears that with further mechanical optimization much higher values of UAV_R^{-1} can be obtained at equal ϵ.

Conclusion

Single-phase fluid–rotor heat-transfer coefficients in a three-stage stator–rotor–stator spinning disc reactor are presented as a function of rotor angular velocities (ω=0−157 rad s^{-1}) and volumetric throughflow rates (ϕ_v=15−20 $\cdot$ 10^{-6} m^{3}s^{-1}). Experimentally obtained steady-state outlet temperatures are fitted to a heat-transfer model (based on the heat-transfer model presented by De Beer et al. [17]) to yield values of the heat-transfer coefficient. The values of h_r are independent of ϕ_v and increase from h_r= 0.95 to 34 kWm^{-2}K^{-1} by increasing ω from 0 to 157 rad s^{-1}. The overall heat-transfer coefficient increases with increasing ω as well, up to 8.3 kWm^{-2}K^{-1} at $\omega = 157$ rad s^{-1} (where U_r is mainly limited by conduction through the rotor). The specific energy input rate (i.e., the energetic costs of increasing h_r) increases from ϵ=0.02 to 3.9 MWm$_L^{-3}$ by increasing ω from 0 to 157 rad s^{-1}. This is mainly caused by the dissipation of energy from the rotor. The energetic contribution of the pressure drop is negligible for the current operating conditions.

The fluid–rotor Nusselt number is used to compare the currently obtained values of h_r to literature data. For $Re_\omega \leq 1.1 \cdot 10^5$ a laminar regime is observed (described by Eq. 17), for $Re_\omega \geq 2.3 \cdot 10^5$ the values of Nu_r reach turbulent levels and are described by Eq. 19. This transition from laminar to turbulent for Nu_r is observed to occur at higher values of Re_ω than for Nu_s. In literature turbulence is indeed observed at lower values of Re_ω at the stator than at the rotor.[30,31] It is concluded that, for engineering purposes, the single-phase heat-transfer in spinning disc reactors are described by Eqs. 17 and 19. Equations 17 and 19 are in relatively good agreement (35% and 15% lower, respectively) with correlations presented for heat-transfer in an enclosed rotating disc,[24] given the uncertainty associated with comparing air and water as heat-transfer fluids.

The convective heat-transfer coefficients obtained in the srs-SDR are a factor 2–3 higher than values achievable in passively enhanced reactor-heat exchangers (e.g., plate and plate fin heat exchangers). This is due to 1–2 orders of magnitude larger specific energy input achievable in the srs-SDR, without requiring a prohibitively high pressure drop. Moreover, as h_r is independent of ϕ_v, the heat-transfer rates in the srs-SDR are independent of residence time. Although the values of UAV_R^{-1} obtained in the current setup are comparable to what is achievable in compact heat exchangers at lower ϵ, it is expected that with further mechanical optimization this value can be increased at least a factor 3. Together with the high mass-transfer rates reported for spinning disc reactors[18–20] this makes it a promising tool to intensify heat-transfer rates for fast, highly exothermal chemical reactions.

Notation

Latin symbols

A = heat-transfer area, m^2
a_i = coefficients for PHE, Eqs. A8 and A10, i=1−6
b_i = geometry coefficients for PFH, Eqs. A11 and A12, i=1−3
c = proportionality constant, Eqs. 1 and 2
c_p = heat capacity at constant pressure, Jkg^{-1}K^{-1}
d = width, m
d_h = hydraulic diameter, m
E_{dp} = energy dissipation rate due to pressure drop, W
E_{dr} = energy dissipation rate per stage due to rotation, W
E_{loss} = rate of energy loss to the environment, W
g = standard gravitational acceleration, ms^{-2}
H = enthalpy, Jkg^{-1}
h = convective heat-transfer coefficient, Wm^{-2}K^{-1}
I = current, A
I_0 = internal current losses, A
I_c = nominal current motor, A
k = thermal conductivity, Wm^{-1}K^{-1}
L = reactor length, m
P = pressure, Pa
Q = heat-transfer rate, W
r = radius, m
s = axial rotor–stator gap, m

t = time, s
T = temperature, K
U = overall heat-transfer coefficient, $Wm^{-2}K^{-1}$
V = volume, m^3
v = velocity, ms^{-1}
x = height, m

Greek symbols

β = corrugation angle in PHE, degrees
Δ = finite difference
Δr_s = radial rotor–stator gap, m
ϵ = specific energy input rate, Wm_L^{-3}
η = heat exchange effectiveness
ν = kinematic viscosity, m^2s^{-1}
ρ = density, kg m^{-3}
τ = torque, Nm
τ_c = torque constant motor, NmA^{-1}
τ_m = mean residence time, $V_R \phi_v^{-1}$, s
ϕ_v = volumetric throughflow, m^3s^{-1}
ψ = effective to projected surface ratio in PHE, -
ω = angular velocity, rad s^{-1}

Dimensionless numbers

C_w = superposed dimensionless throughflow rate, $\phi_v r^{-1} \nu^{-1}$
f_F = Fanning friction factor
G = gap ratio, sr^{-1}
j = Colburn j-factor
Nu = Nusselt number, $hr_{r,2}k_f^{-1}$
Nu_d = Nusselt number, $hd_h k_f^{-1}$
Pr = Prandtl number, $\nu \rho c_p k_f^{-1}$
Re_d = Reynolds number, $vd_h \nu^{-1}$
Re_ω = rotational Reynolds number, $\omega r^2 \nu^{-1}$

Subscripts

1 = lower boundary of heat-transfer area
2 = upper boundary of heat-transfer area
air = air
f = fluid
i = inner side (at the shaft)
in = inlet
k = index (stirred tank of exterior cavity)
L = liquid
m = index (stirred tank of interior cavity)
max = maximum
n = index (stirred tank, opposite m or k on other side of stator)
o = outer side (at the rim)
out = outlet
r = rotor
R = reactor
s = stator
T = total
trans = transition
w = wall
water = water

Superscripts

ext = exterior cavity
int = interior cavity
lam = laminar regime
trans = laminar-turbulent transition regime
turb = turbulent regime

Abbreviations

PFH = plate fin heat exchangers
PHE = plate heat exchangers
SDR = spinning disc reactor
srs-SDR = stator-rotor-stator spinning disc reactor
rs-SDR = rotor-stator spinning disc reactor

Acknowledgment

This project takes places within the ISPT (Institute for Sustainable Process Technology) framework. The authors are grateful to D. Bindraban for the technical design of the stator–rotor–stator spinning disc reactor.

Literature Cited

1. Phillips CH, Lauschke G, Peerhossaini H. Intensification of batch chemical processes by using integrated chemical reactor-heat exchangers. *Appl Therm Eng.* 1997;17:809–824.
2. Dautzenberg FM, Mukherjee M. Process intensification using multifunctional reactors. *Chem Eng Sci.* 2001;56:251–267.
3. Westerterp K, Molga E. Safety and runaway prevention in batch and semibatch reactors - A review. *Chem Eng Res Des.* 2006;84:543–552.
4. Anxionnaz Z, Cabassud M, Gourdon C, Tochon P. Heat exchanger/reactors (HEX reactors): Concepts, technologies: State-of-the-art. *Chem Eng Process: Process Intensification.* 2008;47: 2029–2050.
5. Brechtelsbauer C, Ricard F. Reaction engineering evaluation and utilization of static mixer technology for the synthesis of pharmaceuticals. *Org Process Res Dev.* 2001;5:646–651.
6. Commenge JM, Falk L, Corriou JP, Matlosz M. Analysis of microstructured reactor characteristics for process miniaturization and intensification. *Chem Eng Technol.* 2005;28:446–458.
7. Prat L, Devatine A, Cognet P, Cabassud M, Gourdon C, Elgue S, Chopard F. Performance evaluation of a novel concept Open Plate Reactor applied to highly exothermic reactions. *Chem Eng Technol.* 2005;28:1028–1034.
8. Ferrouillat S, Tochon P, Valle DD, Peerhossaini H. Open loop thermal control of exothermal chemical reactions in multifunctional heat exchangers. *Int J Heat Mass Transfer.* 2006;49:2479–2490.
9. Ferrouillat S, Tochon P, Garnier C, Peerhossaini H. Intensification of heat-transfer and mixing in multifunctional heat exchangers by artificially generated streamwise vorticity. *Appl Therm Eng.* 2006;26: 1820–1829.
10. Shah RK, Focke WW. Plate heat exchangers and their design theory. In: Shah RK, Subbarao E, Mashelkar RA, editor. *Heat Transfer Equipment Design*. Washington, DC: Hemisphere Publishing Co., 1988:227–254.
11. Wang L, Sunden B, Manglik R. *Plate Heat Exchangers: Design, Applications and Performance*, 1st ed. Southampton, WIT Press, 2007.
12. Manglik RM, Bergles AE. Heat transfer and pressure drop correlations for the rectangular offset strip fin compact heat exchanger. *Exp Therm Fluid Sci.* 1995;10:171–180.
13. Kraus A, Aziz A, Welty J. *Extended Surface Heat Transfer*, 1st ed. New York, NY: Wiley, 2001.
14. Kakac S, Shah RK, Bergles AE. *Low Reynolds Number Flow Heat Exchangers*, 1st ed. Washington, DC: Hemisphere Publishing Co., 1983.
15. Boomsma K, Poulikakos D, Zwick F. Metal foams as compact high performance heat exchangers. *Mech Mater.* 2003;35:1161–1176.
16. Ramshaw C. The opportunities for exploiting centrifugal fields. *Heat Recovery Syst CHP.* 1993;13:493–513.
17. De Beer MM, Pezzi Martins Loane L, Keurentjes JTF, Schouten JC, Schaaf J. Single phase fluid-stator heat-transfer in a rotor-stator spinning disc reactor. *Chem Eng Sci.* 2014b;119:88–98.
18. Meeuwse M, Schaaf J, Schouten JC. Mass transfer in a rotor-stator spinning disk reactor with cofeeding of gas and liquid. *Indus Eng Chem Res.* 2010;49:1605–1610.
19. Visscher F, Schaaf J, Croon M, Schouten JC. Liquid-liquid mass transfer in a rotor-stator spinning disc reactor. *Chem Eng J.* 2012; 185-186:267–273.
20. Meeuwse M, Lempers S, Schaaf J, Schouten JC. Liquid-solid mass transfer and reaction in a rotor-stator spinning disc reactor. *Ind Eng Chem Res.* 2010b;49:10751–10757.
21. De Beer MM, Keurentjes JTF, Schouten JC, Schaaf J. Engineering model for single-phase flow in a multi-stage rotor-stator spinning disc reactor. *Chem Eng J.* 2014;242:53–61.

22. Harmand S, Watel B, Desmet B. Local convective heat exchanges from a rotor facing a stator. *Int J Therm Sci*. 2000; 39:404–413.
23. Peev G, Peshev D, Nikolova A. Gas absorption in a thin liquid film flow on a horizontal rotating disk. *Heat Mass Transfer*. 2007;43: 843–848.
24. Nikitenko N. Experimental investigation of heat exchange of a disk and a screen. *J Eng Phys*. 1963;6:1–11.
25. Daily JW, Nece RE. Chamber dimension effects on induced flow and frictional resistance of enclosed rotating disks. *J Basic Eng*. 1960;82:217–232.
26. Green D, Perry R. *Perry's Chemical Engineers' Handbook*, *8th ed*. New York, NY: McGraw-Hill, 2007.
27. Bird RB, Stewart WE, Lightfoot EN. *Transport Phenomena*, *2nd ed*. Hoboken, NJ: Wiley, 2007.
28. Kapinos VM. Heat transfer from a disc rotating in a housing with a radial flow of coolant. *J Eng Phys Thermophys*. 1965;8:35–38.
29. Poncet S, Schiestel R. Numerical modeling of heat-transfer and fluid flow in rotor-stator cavities with throughflow. *Int J Heat Mass Transfer*. 2007;50:1528–1544.
30. Itoh M, Yamada Y, Imao S, Gonda M. Experiments on turbulent flow due to an enclosed rotating disk. *Exp Therm Fluid Sci*. 1992;5: 359–368.
31. Cheah S, Iacovides H, Jackson D, Ji H, Launder BE. Experimental investigation of enclosed rotor-stator disk flows. *Exp Therm Fluid Sci*. 1994;9:445–455.
32. Millsaps K, Pohlhausen K. Heat transfer by laminar flow from a rotating plate. *J Aeronaut Sci*. 1952;19:120–126.
33. Cobb EC, Saunders OA. Heat transfer from a rotating disk. *Proc R Soc London Series A, Math Phys Sci*. 1956;236:343–351.
34. Owen JM, Rogers RH. *Flow and Heat Transfer in Rotating-Disc Systems. Vol.1: Rotor-Stator Systems*, 1st ed. Taunton, UK: Wiley, 1989.
35. Dorfman LA. *Hydrodynamic Resistance and Heat Loss of Rotating Solids*, *1st ed*. Edinburg, UK: Oliver and Boyd, 1963.
36. Lygren M, Andersson HI. Turbulent flow between a rotating and a stationary disk. *J Fluid Mech*. 2001;426:297–326.
37. Cros A, Le Gal P. Spatiotemporal intermittency in the torsional Couette flow between a rotating and a stationary disk. *Phys Fluids*. 2002;14:3755–3765.
38. Popiel C, Boguslawski L. Local heat-transfer coefficients on the rotating disk in still air. *Int J Heat Mass Transfer* 1975;18:167–170.
39. Mohr CM, Newman J. Mass transfer to a rotating disk in transition flow. *J Electrochem Soc*. 1976;123:1687–1691.
40. Cardone G, Astarita T, Carlomagno GM. Heat transfer measurements on a rotating disk. *Int J Rotating Machinery*. 1997;3:1–9.
41. Shchukin V, Olimpiev V. Heat transfer of disc rotating in a housing with transitional and turbulent boundary layers. *Izvestiya VUZ. Aviatsionnaya Tekhnika*. 1975;18:105–110.
42. Meeuwse M, Schaaf J, Schouten JC. Multistage rotor-stator spinning disc reactor. *AIChE J*. 2012;58:247–255.
43. Horve LA. *Shaft Seals for Dynamic Applications*, *1st ed*. New York, NY: Marcel Dekker, 1996.
44. Lu X, Khonsari MM, Gelinck ERM. The Stribeck curve: Experimental results and theoretical prediction. *J Tribol*. 2006;128:789.
45. Debuchy R, Dyment A, Muhe H, Micheau P. Radial inflow between a rotating and a stationary disc. *Eur J Mech - B/Fluids*. 1998;17: 791–810.
46. Poncet S, Chauve MP, Schiestel R. Batchelor versus Stewartson flow structures in a rotor-stator cavity with throughflow. *Phys Fluids*. 2005;17:075110.
47. Poncet S, Schiestel R, Chauve MP. Centrifugal flow in a rotor-stator cavity. *J Fluids Eng*. 2005b;127:787.
48. Blasius PRH. Das Aehnlichkeitsgesetz bei Reibungsvorgangen in Flüssigkeiten. *Forschungsheft*. 1913;131:1–41.
49. Janssen L, Warmoeskerken M. *Transport Phenomena Data Companion*, *3rd ed*. Delft, NL: Delft University Press, 2001.
50. Calderbank PH, Moo-Young MB. The continuous phase heat and mass transfer properties of dispersions. *Chem Eng Sci*. 1961;16:39–54.
51. Landahl MT, Mollo-Christensen E. *Turbulence and Random Processes in Fluid Mechanics*, *2nd ed*. Cambridge, UK: Cambridge University Press, 1992.
52. Coulson JM, Richardson JF, Backhurst JR, Harker JH. *Chemical Engineering. Vol.1: Fluid Flow, Heat Transfer and Mass Transfer*, *6th ed*. Oxford, UK: Elsevier, 1999.
53. Munro R. Material properties of a sintered α-SiC. *J Phys Chem Ref Data* 1997;26:1195–1203.
54. Trambouze P, Euzen JP. *Chemical Reactors from Design to Operation*, *1st ed*. Paris: Editions Technip, 2004.
55. Graetz L. Über der warmeleitungsfähigkerten der flussigkeiten. *Annalen der Physik*. 1883;18:79–94.
56. Colburn AP. A method for correlating forced convection heat-transfer data and a comparison with fluid friction. *Trans Am Inst Chem Eng* 1933;29:174–210.
57. Sieder EN, Tate GE. Heat transfer and pressure drop of liquids in tubes. *Ind Eng Chem*. 1936;28:1429–1435.
58. Muley A, Manglik R. Experimental study of turbulent flow heat-transfer and pressure drop in a plate heat exchanger with chevron plates. *J Heat Transfer*. 1999;121:110–117.
59. Muley A, Manglik RM, Metwally HM. Enhanced heat-transfer characteristics of viscous liquid flows in a chevron plate heat exchanger. *J Heat Transfer*. 1999;121:1011–1017.

Appendix : A Thermo-Hydraulic Correlations

Figure 9 displays the convective heat-transfer coefficient in tubular, plate and plate fin reactor-heat exchangers as function of their specific energy dissipation. This appendix presents the used correlations for these reactors. The correction for viscosity was equal for all used correlations for Nu_d and therefore not taken into account. The value of h is determined by:

$$h=\frac{\mathrm{Nu}_d k_f}{d_h} \tag{A1}$$

while the specific energy dissipation is calculated according to[27]:

$$\epsilon=\frac{\Delta P \phi_v}{V_L}=2\rho v^3 f_F d_h^{-1} \tag{A2}$$

The Fanning friction factor for tubular flow (with $d_h=d=10 \cdot 10^{-3}$ m [52,54]) is obtained by[48,27]:

$$f_F=\frac{16}{\mathrm{Re}_d}; \quad \mathrm{Re}_d < 2.1 \cdot 10^3 \tag{A3}$$

$$f_F=\frac{0.079}{\mathrm{Re}_d^{1/4}}; \quad 2.1 \cdot 10^3 < \mathrm{Re}_d < 10^5 \tag{A4}$$

The Nusselt number for flow in tubes[55–57]:

$$\mathrm{Nu}_d=3.66; \quad \mathrm{Re}_d < 2.1 \cdot 10^3 \tag{A5}$$

$$\mathrm{Nu}_d=0.023\mathrm{Re}_d^{\frac{4}{5}}\mathrm{Pr}^{\frac{1}{3}}; \quad \mathrm{Re}_d > 10^4 \tag{A6}$$

The value of f_F for plate heat exchangers (with $d_h=2 \cdot 1.50 \cdot 10^{-3}$ m, $\beta=45^{\circ}$, $\psi=1.29$[11]) is obtained by[58,59]:

$$f_F=\left[\left(\frac{30.20}{\mathrm{Re}_d}\right)^5+\left(\frac{6.28}{\mathrm{Re}_d^{0.5}}\right)^5\right]^{0.2}\left(\frac{\beta}{30}\right)^{0.83} 2 < \mathrm{Re}_d < 300 \tag{A7}$$

$$f_F=a_1 a_2 \mathrm{Re}_d^{-a_3} \quad \mathrm{Re}_d > 10^3 \tag{A8}$$

The Nusselt number for plate heat exchangers[58,59]:

$$\mathrm{Nu}_d=1.6774\left(\frac{d_h}{L}\right)^{0.13}\left(\frac{\beta}{30}\right)^{0.38}\mathrm{Re}_d^{0.5}\mathrm{Pr}^{\frac{1}{3}} \quad 30 < \mathrm{Re}_d < 400 \tag{A9}$$

$$\mathrm{Nu}_d = a_4 a_5 \mathrm{Re}_d^{a_6} \mathrm{Pr}^{\frac{1}{3}} \quad \mathrm{Re}_d > 10^3 \tag{A10}$$

with:

$$a_1 = 2.917 - 0.1277\beta + 2.016 \cdot 10^{-3}\beta^2$$

$$a_2 = 5.474 - 19.02\psi + 18.93\psi^2 - 5.341\psi^3$$

$$a_3 = 0.2 + 0.0577\sin\left[\left(\frac{\pi\beta}{45}\right) + 2.1\right]$$

$$a_4 = 0.2668 - 0.006967\beta + 7.244 \cdot 10^{-5}\beta^2$$

$$a_5 = 20.78 - 50.94\psi + 41.16\psi^2 - 10.51\psi^3$$

$$a_6 = 0.728 + 0.0543\sin\left[\left(\frac{\pi\beta}{45}\right) + 3.7\right]$$

The value of f_F and j for plate fin heat exchangers (with $d_h = 2 \cdot 10^{-3}$ m, $b_1 = 0.6$, $b_2 = 0.19$, $b_3 = 0.1$[8]) is obtained by[12]:

$$f_F = 9.6243\mathrm{Re}_d^{-0.7422} b_1^{-0.1856} b_2^{0.3053} b_3^{-0.2659} \cdot \ldots$$
$$\ldots \cdot \left[1 + 7.669 \cdot 10^{-8}\mathrm{Re}_d^{4.429} b_1^{0.920} b_2^{3.767} b_3^{0.236}\right]^{0.1}; \tag{A11}$$
$$300 < \mathrm{Re}_d < 10^4$$

$$j = 0.6522\mathrm{Re}_d^{-0.5403} b_1^{-0.1541} b_2^{0.1499} b_3^{-0.0678} \cdot \ldots$$
$$\ldots \cdot \left[1 + 5.269 \cdot 10^{-5}\mathrm{Re}_d^{1.340} b_1^{0.504} b_2^{0.456} b_3^{-1.055}\right]^{0.1}; \tag{A12}$$
$$300 < \mathrm{Re}_d < 10^4$$

with: $\mathrm{Nu}_d = j\mathrm{Re}_d\mathrm{Pr}^{1/3}$

Manuscript received Dec. 2, 2014, and revision received Feb. 10, 2015.